

Experimental and numerical study about seismic retrofitting of corrosion-damaged reinforced concrete columns of bridge using combination of FRP wrapping and steel profiles

Hassan Afshin^{*}, Mohammad R. Nouri Shirazi^a and Karim Abedi^b

Department of Civil Engineering, Sahand University of Technology, Tabriz, Iran

(Received April 17, 2018, Revised December 20, 2018, Accepted January 31, 2019)

Abstract. In the present study, a numerical and experimental investigation has been carried out on the seismic behavior of RC columns of a bridge which damaged under corrosive environments and retrofitted by various techniques including combined application of CFRP sheets and steel profiles. A novel hybrid retrofitting procedure, including the application of inner steel profiles and outer peripheral CFRP sheets, has been proposed for strengthening purpose. Seven large-scale RC columns of a Girder Bridge have been tested in the laboratory under the influence of simultaneous application of constant axial load and the lateral cyclic displacements. Having verified the finite element modeling, using ABAQUS software, the effects of important parameters such as the corrosion percentage of steel rebars and the number of CFRP layers have been evaluated. Based on the results, retrofitting of RC columns of the bridge with the proposed technique was effective in improving some measures of structural performance such as lateral strength degradation and higher energy absorption capability. However, the displacement ductility was not considerably improved whereas the elastic stiffness of the specimens has been increased.

Keywords: seismic retrofitting; RC columns; corrosion; CFRP sheets; steel reinforcement; finite element analysis

1. Introduction

The deterioration caused by the corrosive conditions in RC structures is one of the fundamental problems in civil engineering. The main reason for corrosion phenomenon is the corrosion of steel rods under the influence of chloride penetration into RC members. Two main sources of chlorides in nature affecting structural specifications of bridge RC columns include seawater and deicing chemicals (Andisheh *et al.* 2016, Aquino and Hawkins 2007). Chloride causes additional structural failures due to a reduction of steel rebar cross-section and adhesion reduction at the interface of concrete and steel rebar. Therefore, RC structures damaged by corrosion may exhibit undesirable seismic performance; so that some of these structures have experienced structural failures under strong earthquake conditions (Gong *et al.* 2004, Lee *et al.* 2003, Maaddawy 2008). Many researches on the seismic behavior of corrosion-damaged RC columns have proven that the corrosion significantly affects the overall seismic performance, in particular, a significant reduction in strengths capacities and a noticeable increase in drift ratio (Meda *et al.* 2014, Li *et al.* 2009, Goksu 2012, Ranjith *et al.* 2016, Husain *et al.* 2017, Gao *et al.* 2016, 2017, Chen and

Xiao 2015, Greco and Marano 2015, Anoop and Rao 2015, Malerba *et al.* 2017). The RC column, which is considered as the main structural member of the bridge structure, is subjected to gravity forces, including dead and live loads. When the earthquake happens, they may be repeatedly subjected to flexural moments and shear forces. However, in some cases these members suffer a brittle shear failure or failures due to the destroying of adhesion between the concrete and the steel interface (AIJ 1987, Nakayama *et al.* 1995). Therefore, it is necessary to study the effects of using an efficient technique for strengthening of corrosion-damaged RC columns and improving their seismic performance. The FRP sheets are ideal polymer products which can be used as retrofitting materials for damaged or poorly designed RC columns. This technique is used in two general fields of application, including rehabilitation and retrofitting of RC columns. This method has various advantages which are ideal as an alternative to other conventional retrofitting and rehabilitation techniques (Pantazopoulou *et al.* 2001). The studies have demonstrated that using of FRP sheets in the form of lateral confinement elements improve seismic characteristics including ductility, energy absorption and shear strength of RC columns. However, when the FRP sheet is used in the longitudinal direction of RC member, it can also improve the flexural strength.

One of the most conventional retrofitting techniques used in the past was the confinement of RC members using steel jacketing. The use of this system improves the flexural strength, shear strength, elastic stiffness, ductility and axial load carrying capacity of the retrofitted members (Lu *et al.*

^{*}Corresponding author, Ph.D., Associate Professor,
E-mail: hafshin@sut.ac.ir

^aPh.D. Candidate of Structural Engineering,
E-mail: mrns1981@gmail.com

^bPh.D., Professor, E-mail: k_abedi@sut.ac.ir

2005, Sheikh and Yau 2002, Vadoros and Dritsos 2008, Abdullah and Katsuki 2003, Adam *et al.* 2008, 2009, Badalamenti *et al.* 2010, Barga *et al.* 2006, Campione 2012, Montuori and Piluso 2009, Ramirez *et al.* 1997). However, in marine environments and de-icing salt conditions, the steel jacket is not convenient for rehabilitation of the corroded RC columns considering progressive corrosion conditions. As proved in the past, both of longitudinal and transverse reinforcements (Ma *et al.* 2012) are vulnerable to corrosion in damaged-corrosion RC columns; however, their flexural and shear strength capacity should be enhanced. Very little efforts have been made for retrofitting of corroded RC bridge columns using simultaneous application of two different types of materials for improving their seismic performance. In general, the studies have been carried out mainly on the building columns or a field study on a particular bridge. Li *et al.* (2009) conducted a comprehensive investigation into the effects of the simultaneous application of CFRP sheets and steel jackets on the behavior of rehabilitated RC columns with rectangular cross-section under the simultaneous application of constant axial load and reversed cyclic displacements. They demonstrated that the retrofitting operations were effective in improving the seismic performance of the retrofitted RC columns. Choi *et al.* (2011) proposed a method for the overturning problem and tensile cracking development of a railroad bridge columns using simultaneous application of CFRP wraps and steel plates. The results proved that the installed anchors in the ground were effective in preventing the overturning problem of the column. The FSPs and the FRP strips prevented the cracking of the concrete and increased the flexural strength (Choi *et al.* 2011). The behavior of corrosion-damaged RC bridge columns subjected to earthquake loading has been rarely investigated before. Furthermore, the retrofitting feasibility of corroded RC columns using a composite of CFRP wraps and steel elements has been limited to only small-scale laboratory experiments. Therefore, this study presents a retrofitting plan for corrosion-damaged large scale RC bridge columns in the laboratory to enhance the seismic performance. Moreover, the FEM technique has been used for better understanding of the structural behavior of retrofitted RC columns using commercial software, ABAQUS. Therefore, the objectives of the present research are as follows:

- (1) The investigation into the efficiency of different hybrid retrofitting techniques and comparison with the proposed technique;
- (2) Study about the effects of important parameters including the corrosion rate of steel rebar and the number of CFRP layers.

2. Experimental study

2.1 Specimen details

In the experimental part of the present study, the specifications of a RC bridge column of Tehran-Chalus freeway Girder Bridge was considered and used for scaling.

Based on the dimensions of the test loading setup, the scale factor 1/7 was considered and the concepts presented by Yu *et al.* (1989) have been applied for the scaling. Seven identical large scale RC columns were constructed and tested under the influence of both axial load and cyclic lateral displacements. As illustrated in Fig. 1, the initial RC column is divided into three parts. Moreover, the implemented concrete cover was 25 mm. The lower part, RC footing, was constructed using rebars of 12-mm diameter as longitudinal and stirrups. The cap beam had rebars of 12-mm diameter as longitudinal and stirrups. Three 150×150×150 mm concrete cubes were constructed in the laboratory which the compressive strength in 28-day was 49.53 MPa and 47 MPa for RC footing and both of RC column and cap beam, respectively. In Table 1, the details of the concrete mix are given. The configurations of the test specimens are presented in Table 2. A schematic view of the test specimens is presented in Fig. 2.

Benchmark specimens including C1-BEN-C and C2-BEN-UC have not been retrofitted; however, the other specimens have been strengthened using different techniques. All of the specimens, except C2-BEN-UC, have been damaged in the corrosion process. The detailed specifications of each specimen are presented and discussed in the “repair and strengthening process” section.

2.2 Setup of corrosion

For simulation a corrosive environment within a reasonable time on the six constructed RC bridge columns,

Table 1 Properties of concrete mixing plan

Structural member	Water/cement ratio	Water (kg/m ³)	Cement (kg/m ³)	Fine aggregate (kg/m ³)	Coarse aggregate (kg/m ³)
RC footing	0.49	194.66	400	940	813.33
Columns and cap beam	0.45	180	400	966.66	840

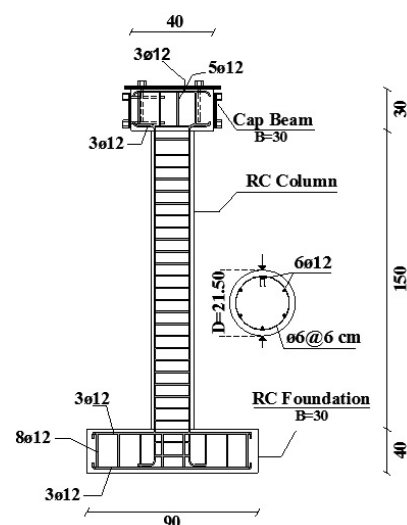


Fig. 1 Geometric schematic of test specimen; (units in cm, B = width of the footing and the cap beam)

Table 2 Configuration of specimens

No. Specimen symbol	Retrofitting Technique	Notes
C1-BEN-C	not retrofitted; corrosion-damaged	benchmark specimen-BEN1
C2-BEN-UC	not retrofitted; un-corroded	benchmark specimen-BEN2
C3-2CF	retrofitted- 2 layer of CFRP sheet; corrosion-damaged	-
C4-SR-2CF	retrofitted- steel rods+2 layer of CFRP sheet; corrosion-damaged	NSM reinforcement
C5-BP-2CF	retrofitted- steel strips+2 layer of CFRP sheet; corrosion-damaged	proposed technique-PT1
C6-CF-BP-CF	retrofitted- 1 layer of CFRP sheet+steel strips+1 layer of CFRP sheet; corrosion-damaged	proposed technique-PT2
C7-TP-2CF	retrofitted- T shape steel profiles+2 layer of CFRP sheet; corrosion-damaged	proposed technique-PT3

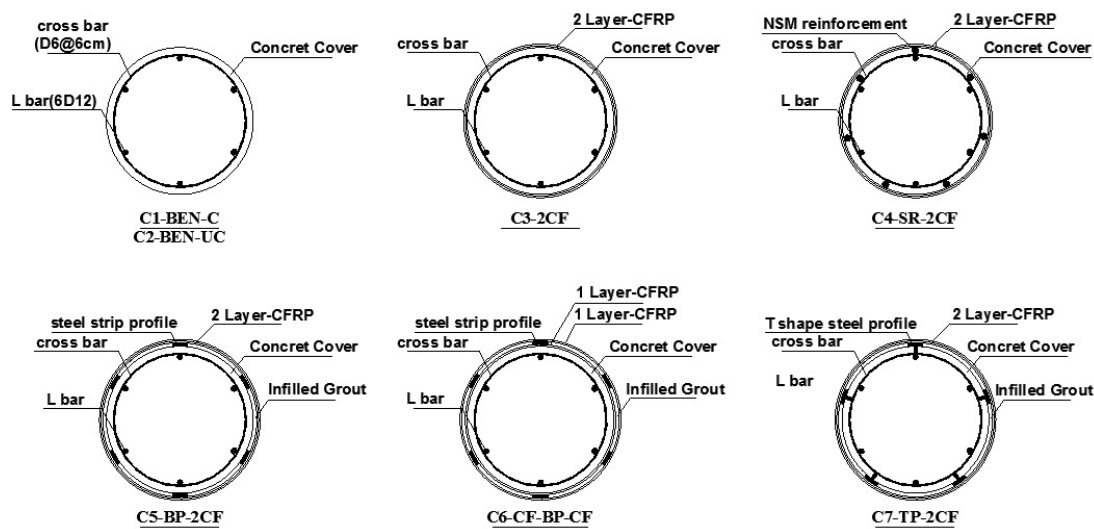


Fig. 2 Cross-sectional plan of the RC columns with their retrofitting plans



Fig. 3 A perspective of accelerated corrosion setup

a simple accelerated corrosion setup has been provided in the laboratory. It is worth noting that the specimens were not retrofitted, and vibrated along the concreting process. The mechanical effects produced around the steel rebars and the cover layer of concrete, including the depletion of steel surface and the accumulation of its rust, are among the conditions difficult to simulate with the electrochemical method. One of the main concerns for better performance of corrosion setup is to provide enough oxygen to the

corrosion cell to produce iron rust, which creates a network of fine cracks on the surface of the RC columns, the same phenomenon that has been observed in nature (Tastani and Pantazopoulou 2004). As shown in Fig. 3, all of the RC column specimens except C2-BEN-UC are placed inside the water tank containing 3% natural salt (Aquino and Hawkins 2007). The presence of oxygen is necessary for the continuation of the corrosion process and includes iron decomposition into ferrous and ferric oxides.

The corrosion conditions have been created for the RC column in semi-immersed water as an ideal state for the development of the chemical process of corrosion (Pantazopoulou *et al.* 2001). In the present study, the height of submerged part of the RC column was considered 90 cm due to provide a localized corrosion conditions. Electrical aquarium pump has been used within the whole time of the corrosion process for injection more oxygen into the water. It is a proved case that the rate of corrosion in water at a temperature of 50°C is ten times faster than in the water at 10 to 20°C (Fookers 1995). This temperature is typical of different regions of the world. In these areas, inappropriate weather condition causes the RC structures to undergo severe corrosion after 12 months from the time of construction (Debaiky *et al.* 2006). By application of two submerged electrical heaters in the water, the temperature has been achieved about 45°C (to accelerate the corrosion process). The temperature is controlled using a submersible thermometer. Moreover, the temperature and humidity percent of surrounded air was increased using water boiling device for modeling of hot and humidity air conditions. The electrochemical method using a standard electric rectifier has accelerated the corrosion process. Also, the longitudinal and transverse reinforcement of each RC column has been considered as anode pole, where an immersed corrosion-resistant steel rod in the water has been worked as cathode pole. The voltage of all specimens was, without any changes, equal to 6V within the corrosion process, connected to anode and cathode. This amount of voltage is enough to generate corrosion products similar to those that occur in nature (Pantazopoulou *et al.* 2001, Lee *et al.* 2000). By reading the established flow rate (in ampere) between the anode pole and the rectifier device, the amount of current is measured in each day. To provide better oxidation conditions during the corrosion process, the columns experienced five days of wetting and two days of drying cycles per each week.

In the drying cycles, blowing of the excess oxygen has been stopped, while that was established during the wetting process to stimulate further oxygen penetration into the concrete cover. However, the water level of the tank was constant in two different cycles. Because of the good quality of concrete and compacting work along the concreting process, the duration for accelerated-corrosion conditioning in laboratory has been selected as twelve months. In the case of limited supply of oxygen, corrosion products are not necessarily as expansions of the steel meshes, but they can be in the form of soft products, blacksmith and water-soluble compounds. As illustrated in Fig. 4, the columns exposed to corrosive conditions have been damaged in the lower area (submerged part of the RC column) while sever damage was observed at installed steel plates on the cap beam surface. A significant amount of red rusts have been observed along the corrosion process in the immersed area of all columns. The results of corrosion phenomena include loss in cross-sectional area and loss of mechanical properties of the reinforcement bars, decrease in bond strength, and loss in concrete strength and its modulus of elasticity (Yuksel 2015). So the remained effects of the corrosion can be considered as a sign of probable deficient in the RC column which can lead to inappropriate seismic behavior. The reduced mass of iron over time (in second) is estimated using the Faraday's equation. This equation assumes a constant rate of reduction in the iron weight. Faraday's law represents that 96487.6 Columbus (one Faraday) of electric charge transfer reduce one gram equivalent weight of the material which exposed under electrochemical reaction. The depleted mass $\Delta W(g)$ is estimated according to the following equation (Pantazopoulou *et al.* 2001).

$$\Delta W(g) = \frac{I.t.A_m}{z.F} \quad (1)$$



Fig. 4 The condition of damages in columns components after corrosion process

Table 3 Mechanical and geometrical specification of reinforcing steel profiles

Profile	Detail of section (mm)	Height (mm)	Yield stress (MPa)	Number of element	Ultimate stress (MPa)
T shape steel profile	26×4 for web and 30×4 for flange	1480	245	5	374
Steel strip profile	30×6	1480	238	6	368
NSM reinforcement	16 (in diameter)	1480	342	6	538

where the A_m is the atomic mass of iron (55.87 g), I is recorded current in the corrosion process, t is the total duration of corrosion process per second, z is the valency of the reaction (usually taken as 2) and F is Faraday's constant [96487.6 Coulombs (g/equivalent)]. After 12 months of conditioning period (31536000 s) and considering a mean of recorded current (0.57 A), the lost mass of RC column is estimated about 5204 gr. Since the mean weight value of the steel cage was 47250 gr, the approximate mass loss ratio of 11% was calculated for each specimen. Based on the Mangat and Elgarf's research (Mangat and Elgarf 1999), this rate of corrosion can reduce the flexural strength of the damaged member.

2.3 Repair and strengthening process

Five of the corroded specimens have been repaired and retrofitted under laboratory conditions. The overall process of repair and retrofitting of columns was removing the damaged concrete from the column surface, cleaning of steel rebars from rust, repair of the surface using normal strength concrete and finally strengthening of the RC column using different retrofitting techniques. The rehabilitated concrete has a compressive strength of 45 MPa.

Five different types of techniques have been used for retrofitting work. The specimens of C1-BEN-C and C2-BEN-UC have been considered as a benchmark and un-retrofitted, but the difference was in the exposure to corrosion environment. For simulation of a common strengthening technique, specimen C3-2CF has been retrofitted using two layers of the CFRP. The NSM retrofitting method includes creating grooves on the concrete surface; embedding of the steel rebars, sticking using resin-epoxy binder and then filling the grooves using low strength concrete (Dionysios *et al.* 2009). This technique is considered as a fundamental solution to improve the flexural strength of RC columns affected by earthquake forces (Sasmal *et al.* 2011). Specimen C4-SR-2CF has been strengthened using NSM technique. Six rebars of 16-mm diameter were installed using resin-epoxy adhesive on the grooved surface of the corroded RC columns considering gap size of 10 mm in the top and bottom of the column. Then two layers of the CFRP sheet have been wrapped around the perimeter of the column cross-section. For the strengthening of specimens C5-BP-2CF and C6-CF-BP-CF, the PT1 and PT2 retrofitting techniques have been implemented, respectively. Therefore, six steel strips (30×6 mm in cross-section and 1480 mm in the height) have been attached on the RC column, using the resin-epoxy binder. For specimen C5-BP-2CF, the steel

Table 4 Mechanical and geometrical specification of CFRP sheets

Thickness, per ply (mm)	Tensile strength (MPa)	Tensile modulus (MPa)	Tensile elongation (%)
0.32	1421	117351	1.6

strips have been mounted firstly on the RC column surface, and the created space has been filled using low strength concrete (concrete specified strength equal to 34 MPa), then two layers of CFRP sheets have been wrapped around the column cross-section using adhesive. These retrofitting elements have been used for specimen C6-CF-BP-CF, but the application order of the retrofitting elements was different. The geometric shape of steel profiles has a considerable effect on the flexural strength of the retrofitted RC column under reverse cyclic displacement. In the same geometric conditions and considering simple implementation, T shape steel profile (TSSP) has the highest amount of moment inertia than the rectangular and circular cross-section steel profiles. For the specimen C7-TP-2CF in which the PT3 retrofitting technique has been implemented, TSSP with dimensions of 26×4 mm for web and 30×4 mm for flange have been used for implementation. Then two layers of CFRP sheet has been attached to the repaired RC column surface as the final layer of retrofitting work. The detail of retrofitting steel profiles and CFRP sheets are given in Tables 3-4, respectively.

After repairing the column surface, five standard vertical grooves with thickness of 5 mm and depth of 26 mm have been created on the column surface without damaging of remained column rebars. The T shape steel profiles have been installed on the surface using the resin-epoxy binder. To have a better structural performance under cyclic displacement, the steel profiles have been attached on the installed steel rods in RC footing using standard welding system. According to retrofitting scheme of the specimen, five or six 16 mm ribbed steel rods have been installed on the upper surface of the RC footing. The overall length of ribbed steel rod was 300 mm, embedded in the footing surface using the resin-epoxy binder (buried length was 150 mm). Several assumptions have been made including (1) the geometrical and material specifications of the original RC column were similar in all specimens; (2) the specimen C1-BEN-C was considered as a benchmark for studying the effect of different retrofitting techniques on the structural behavior; (3) the specimen C2-BEN-UC was not placed in the conditions of corrosion test setup; (4) the

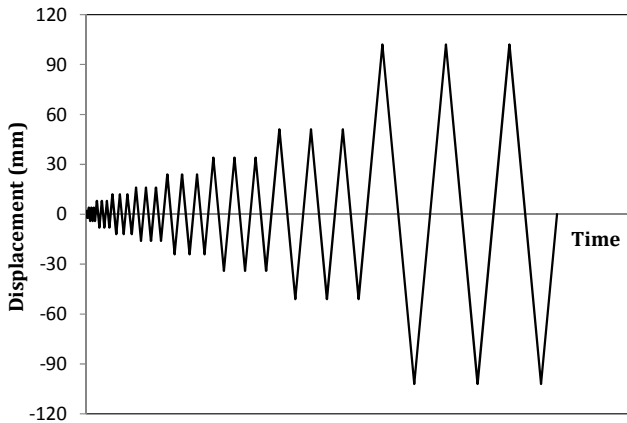


Fig. 7 Typical reverse displacement history adopted for the test

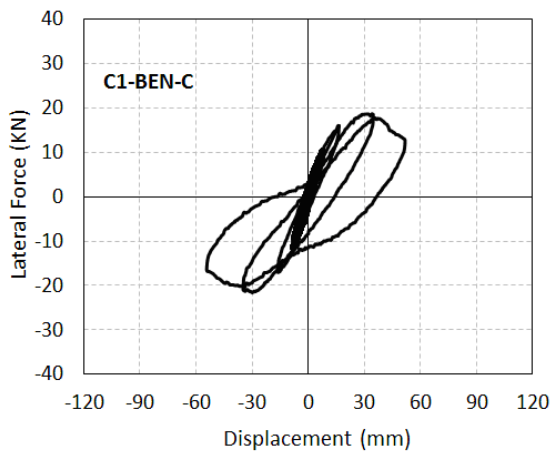
lateral force) with a capacity of 1000 kN, is connected to both of installed actuator and a hinged connection. Also, the load cell has been attached to the cap beam for providing the ability of rotation during the test. After the specimen was set on the place, to model the dead axial load on the bridge column, 12% of column axial load capacity ($0.12f_c A_g$, equal to 200 kN) has been applied firstly using

450-kN two-way hydraulic loading actuator (having a maximum stroke of ± 350 mm) and has been remained constant during the test (f_c and A_g were the compressive strength of concrete and cross-sectional area of the RC column, respectively). The lateral load was applied to all column specimens using a 1000-kN tension-compression hydraulic jack with a maximum stroke of ± 400 mm.

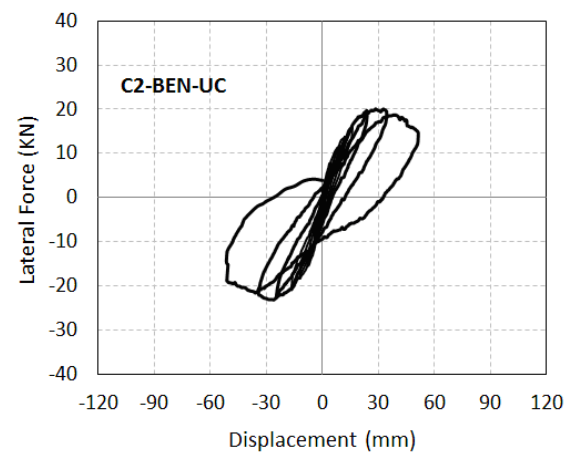
Two standardized LVDT have been installed to record the lateral displacement of the column in the mid-height of the cap-beam and also the displacement values both in loading and unloading modes.

2.5 Loading history

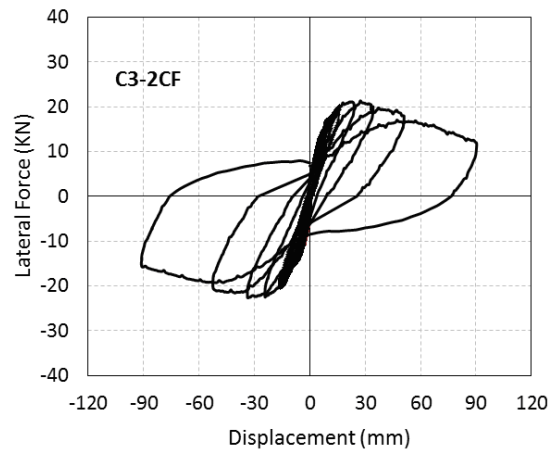
Lateral loading of the test specimens was carried out in a quasi-static manner. The horizontal loads are applied to the columns using a hydraulic jack system controlled by a computer using a shift control method based on an incremental lateral displacement pattern according to Fig. 7. In each amount of displacement, three repetitive cycles consisting of positive and negative displacements have been applied to the columns. The cyclic lateral displacements were applied in the form of the relative displacement ratio (drift ratio) of the column, which is calculated according to the following equation



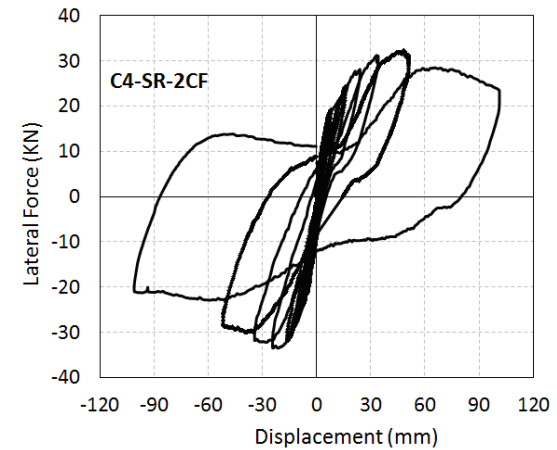
(a) Hysteresis curves of specimen C1-BEN-C



(b) Hysteresis curves of specimen C2-BEN-UC

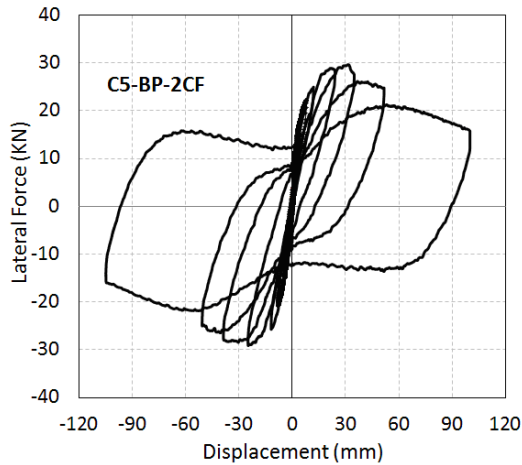


(c) Hysteresis curves of specimen C3-2CF

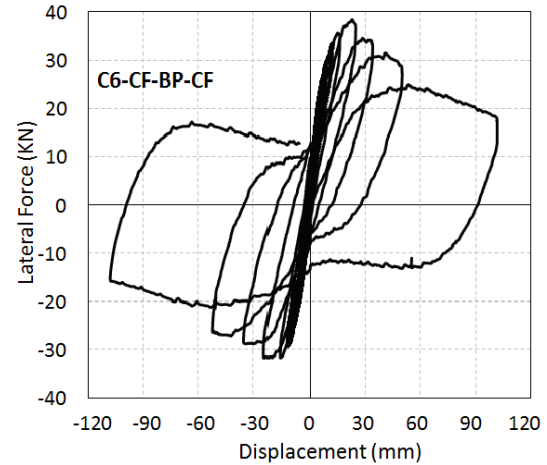


(d) Hysteresis curves of specimen C4-SR-2CF

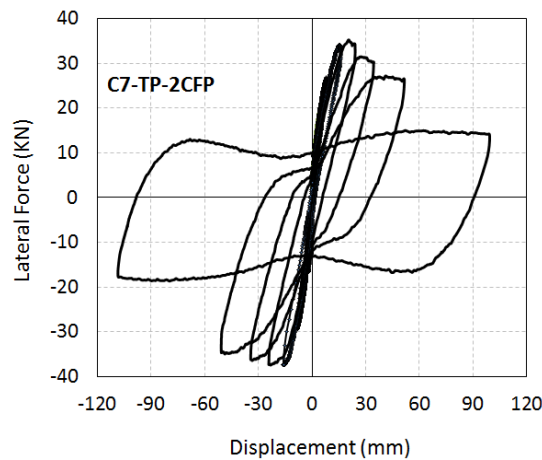
Fig. 8 Lateral force–displacement responses of specimens



(e) Hysteresis curves of specimen C5-BP-2CF



(f) Hysteresis curves of specimen C6-CF-BP-CF



(g) Hysteresis curves of specimen C7-TP-2CF

Fig. 8 Continued

$$D.R(\%) = \frac{\Delta}{h} \times 100 \quad (2)$$

where Δ and h are the displacement applied at the center of the cap beam surface along loading direction and also the distance to the top surface of footing (1650 mm), respectively. The initial displacement was $\Delta_1 = 2.06$ mm corresponding to $0.125D.R$; however, subsequent displacements were increased to $2\Delta_1$; $4\Delta_1$; $6\Delta_1$; $8\Delta_1$; $12\Delta_1$; $16\Delta_1$; $24\Delta_1$; $48\Delta_1$ (Ma *et al.* 2012), until the end of the test loading.

3. Test results

3.1 Cyclic lateral load results

Based on the test results, a comparative investigation were conducted about the effects of rebar corrosion and applying different strengthening techniques on the ductility, load carrying capacity, elastic stiffness and energy absorption capacity. The hysteresis curves in terms of lateral displacement-lateral load have been shown for each of the column specimens in Figs. 8(a)-(g). Two control specimens

BEN1 and BEN2 were tested without any retrofit design, to compare their behaviors with those of the other retrofitted specimens. As illustrated in Figs. 8(a)-(b), the peak shear strength of specimens BEN1 and BEN2 were 18.56 KN and 19.61 KN, respectively, which indicate reduction in strength (about 6%) in the corrosion-damaged specimen. The responses of two specimens were similar in overall; the unsteady hysteresis curves, along with the smaller area observed for damaged columns due to corrosion along the unloading direction. As shown in Fig. 9(a), several small horizontal flexural cracks were observed in the specimen BEN1 before the yield load, however, major horizontal bending cracks have been observed at a distance of approximately 100 mm from each other during subsequent cycles at the bottom of the column. From the fourth cycle, the cracks were propagated down the column and led to the initiation of the process of spalling of the concrete cover near the column-footing interface. In the final cycles of loading, corrosion damage resulted in the spalling of the concrete cover and a decrease in the bond between the concrete cover and the concrete core. The final condition of specimen BEN2 is shown in Fig. 9(b). It is evident that only the bending cracks were formed along the column height, however, the width and number of cracks increased during



(a) Specimen BEN1 at failure



(b) Specimen BEN2 at failure



(c) Specimen C3-2CF at failure



(d) Specimen C4-SR-2CF at failure



(e) Specimen C5-BP-2CF at failure



(f) Specimen C6-CF-BP-CF at failure



(g) Specimen C7-TP-2CF at failure

Fig. 9 Views of columns failure

the final cycles. The lateral displacement-lateral force response for specimen C3-2CF is shown in Fig. 8(c). The peak shear strength and corresponding lateral displacement were 21.01 kN and 26.87 mm, respectively; however, the peak lateral strength was increased after the retrofitting process. The specimen is characterized by a well-defined yield and stable hysteresis curves on both directions of loading; however, degradation of strength began after the sixth cycle of loading and continued until the end cycles. An increase in the rate of circumferential strain is a sign of the volumetric expansion of the concrete caused by progressive damage accumulation. The expansion was due to the high longitudinal compressive stresses for the compression side.

However, for the tension side, the circumferential strains have been increased due to the concrete splitting and the mechanical locking of rebar lugs with surrounding concrete (Aquino and Hawkins 2007). As shown in Fig. 9(c), the specimen C3-2CF has suffered several horizontal flexural cracks. In the fourth cycle of loading, failure of the column initiated with the appearance of horizontal bending cracks in the area near the base of the column. The cracks propagated along the column height by increasing the lateral displacement, but the form of the cracks has not changed due to the presence of the CFRP sheets. Near the column-footing interface, the CFRP sheets were ruptured during the ninth cycle which is an indication of a significant reduction in the flexural strength of the column.

Subsequently, the column loading process was stopped, and the test has been finished. The specimen C4-SR-2CF has been strengthened with combined application of steel rods and CFRP wraps. The steel rods were effective only to enhance the flexural strength of specimen; however, it hadn't any influence on the concrete core confinement. The hysteresis curves of the specimen C4-SR-2CF are shown in Fig. 8(d). The general form of hysteresis curves is similar to those of specimen C3-2CF. The peak shear strength and corresponding lateral displacement are 31.86 KN and 45.64 mm, respectively. The behavior of the column in both loading directions has been stable towards a gradual reduction of strength due to the confinement effect of the CFRP sheets; however, degradation of strength was initiated at cycle 8 and continued until the end of the test. As shown in Fig. 9(d), the specimen had several horizontal flexural cracks. During the fifth cycle, damage of the column was initiated with the appearance of horizontal flexural cracks at the end of the column. When the amount of lateral displacement increases, the number of cracks will increase in the column height. Then the CFRP sheet was ruptured near the base of the column during the ninth cycle. However, under the condition of reversed cyclic displacement, the created loading moments resulted in forming of wedge cracks on the surface of RC footing (considering no strengthened footing) (Aquino and Hawkins 2007). The main reason was the higher elastic stiffness of the retrofitted column than that of the RC footing. It should be noted that this condition was similar for all of specimens C4-SR-2CF, C5-BP-2CF, C6-CF-BP-CF and C7-TP-2CF. The connection was destroyed between the steel rods and the concrete surface near the column–footing interface, causing a noticeable drop in the column flexural strength (Aquino and Hawkins 2007). The other columns that have been retrofitted with simultaneous application of CFRP sheets and steel profiles have the similar behavior. The hysteresis curves of specimens C5-BP-2CF, C6-CF-BP-CF and C7-TP-2CF are illustrated in Figs. 8(e)-(g), respectively. The peak shear strengths of specimens were 29.41 KN, 38.23 KN and 33.95 KN whereas the recorded corresponding lateral displacements were 29 mm, 20.41 mm and 17.89 mm, respectively. Those columns had more stable behavior than the retrofitted specimen using only CFRP sheet (C3-2CF specimen). This stable behavior is due to the confinement effect of CFRP sheets and flexural strength enhancement is due to the use of steel profiles. In an overview, the specimens had stable hysteresis curves in loading and unloading directions; however, the strength degradation of specimens C6-CF-BP-CF and C7-TP-2CF were occurred after the sixth cycle of loading with a steep slope in comparison with that of specimen C4-SR-2CF, whereas this state is started in the seventh cycle of loading for specimen C5-BP-2CF. The achieved peak shear strength of specimens C6-CF-BP-CF and C7-TP-2CF was higher than that of the retrofitted specimen with NSM technique; however, degradation of strength was initiated in the lower cycles. Figs. 9(e)-(f)-(g) illustrates a perspective of specimen's failures after the end of the test. The failure mechanism of all specimens has been affected by the created wedge cracks in the RC footing which was the main

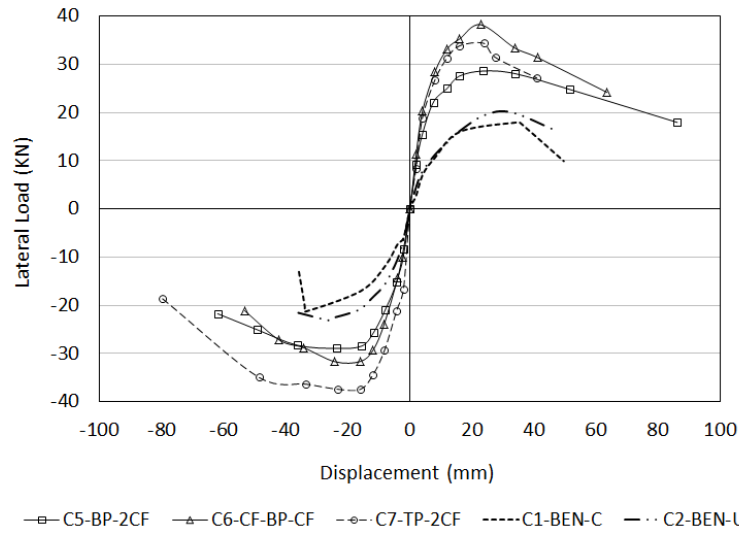
cause of the rapid degradation of hysteresis curves. Damage of the column has initiated during the test process with the formation of horizontal flexural cracks at the end of the column part. The crack is developed along the column height as the lateral displacement increased. Along the final cycle of loading, the CFRP sheet ruptured near the column–footing interface, and afterward, the concrete cover separated from the footing surface. This type of failure was similar for all three mentioned specimens.

3.2 Maximum shear force per lateral displacement curves

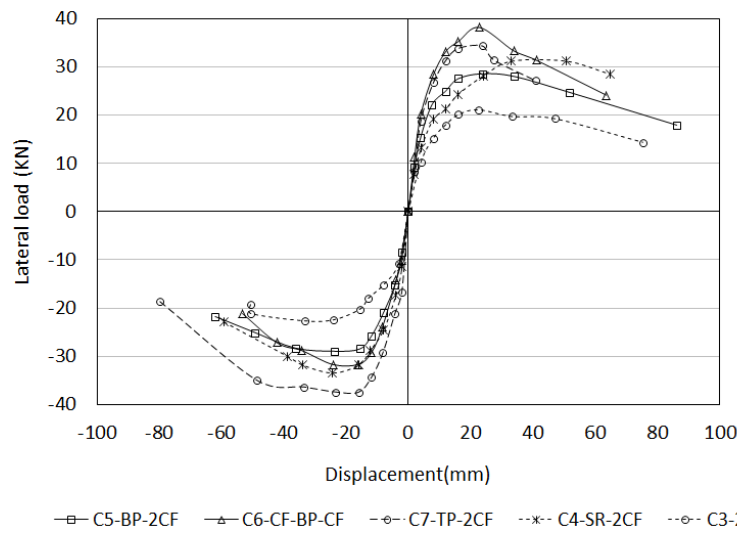
The lateral load–lateral displacement envelope curves derived from the hysteresis curves of the tested columns are considered as an appropriate method for determining the adequacy of the retrofitting techniques. These curves are plotted by selecting the maximum absolute values of shear strength and corresponding lateral displacement in compression and tension loading directions for each cycle of hysteresis curves, as shown in Figs. 10(a)-(b).

For identifying the effectiveness of the used techniques, a comparison was made between the test results of the specimens C5-BP-2CF, C6-CF-BP-CF and C7-TP-2CF against those of the un-retrofitted benchmark RC columns. According to the test results for slightly corroded RC column, specimen BEN1, a slight decrease has been observed in the load carrying capacity and stiffness of the specimen in comparison with the non-corroded benchmark specimen. Corrosion-damaged columns, strengthened with three types of retrofit techniques, have more stable responses and larger shear strength than the other specimens. However, the maximum shear strength for specimen C6-CF-BP-CF was 90% more than of the specimen BEN2 shear strength. In the case of specimen C3-2CF which was strengthened only with CFRP, a small enhancement has been found in the shear strength capacity in comparison with the benchmark specimens.

In any case, confinement of concrete in plastic hinge region using CFRP sheets will increase the bond strength of the corrosion-damaged rebars with concrete, resulted in delaying in the formation of cracks along the length of these rebars. As a result, the lateral load bearing capacity of the columns has improved and the column showed more ductile behavior. The performance of retrofitted specimens with combined strengthening techniques was better than that of the specimen retrofitted by CFRP only, considering larger lateral load carrying capacity. However, the use of steel profiles has improved the flexural strength by increasing the tensile force. In combined strengthening technique, the confinement effect of the CFRP sheets improved the steel profiles adhesion and delayed formation of internal cracks along the length of the steel profiles. Moreover, the possibility of the buckling of the steel profiles was decreased under loading conditions due to the high tensile strength of the CFRP sheets, resulted in improvement of shear strength. The specimens C6-CF-BP-CF and C7-TP-2CF had the best hysteresis behavior compared to other test specimens with more stable hysteresis curves. The influence of higher moment inertia of T-shape steel profiles and



(a) Benchmark specimens in comparison to retrofitted specimens with proposed techniques



(b) Custom retrofitted specimens in comparison to retrofitted specimens with proposed techniques

Fig. 10 Lateral load–lateral displacement envelopes for all specimens

confinement effect of the CFRP layers were the main reasons for this appropriate and better behavior. Some of the tests results are given in Table 5.

Having the yield load (P_y) and corresponding displacement (Δ_y), maximum shear strength of specimen through all cycles (P_{max}) and relevant displacement (Δ_{max}),

ultimate load (P_u) (defined as 85% of the maximum shear strength) and corresponding displacement (Δ_u), the ductility factor based on the lateral displacement-lateral force envelope curves can be calculated for all specimens (Ma *et al.* 2012). The coefficient of displacement ductility can be estimated as

Table 5 Summary of the test results of the column specimens

Specimen	P_y (KN)	Δ_y (mm)	P_{max} (KN)	Δ_{max} (mm)	P_u (KN)	Δ_u (mm)	μ_Δ
C1-Ben-c	15.91	15.90	17.98	35.68	15.28	40.14	2.52
C2-Ben-uc	16.80	15.25	20.05	32.73	17.04	44.19	2.89
C3-2cf	18.36	12.65	21.36	27.38	18.15	52.25	4.13
C4-SR-2cf	26.98	10.22	31.86	23.75	27.08	47.22	4.62
C5-BP-2cf	23.44	10.24	29.67	31.46	25.21	48.67	4.75
C6-CF-BP-CF	27.66	10.29	38.23	22.77	32.49	38.44	3.74
C7-TP-2cf	26.32	10.26	35.23	20.39	29.94	32.45	3.16

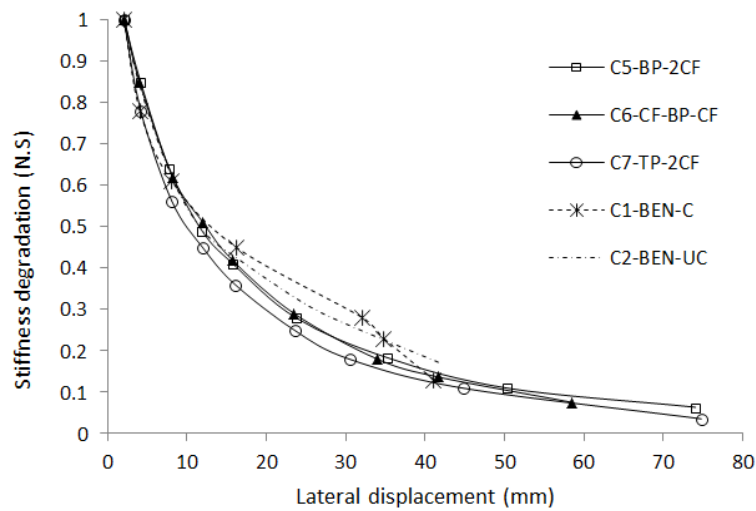
$$\mu_{\Delta} = \frac{\Delta_u}{\Delta_y} \tag{3}$$

For specimen C1-BEN-C, damaged under corrosion conditions, the yield load capacity and ductility factor have been reduced in 5.60% and 14.68% than to those of the uncorroded benchmark specimen (BEN2) which proved the significant influence of the corrosion phenomenon on the structural behavior of the columns. For all of the retrofitted specimens with different confinement techniques, both capacities of yield load and ductility factor were improved. By addition of various steel profiles, the yield and ultimate load carrying capacity were increased significantly. The ductility factor of the specimen C5-BP-2CF was higher than those of the other specimens. This improvement was 64.30%, 15%, and 2.81% more than to the specimens BEN2, C3-2CF and C4-SR-2CF, respectively, whereas the recorded yield load was less than that of specimen C4-SR-2CF. The specimen C6-CF-BP-CF had the highest yield and ultimate load, but the ductility factor has been decreased in

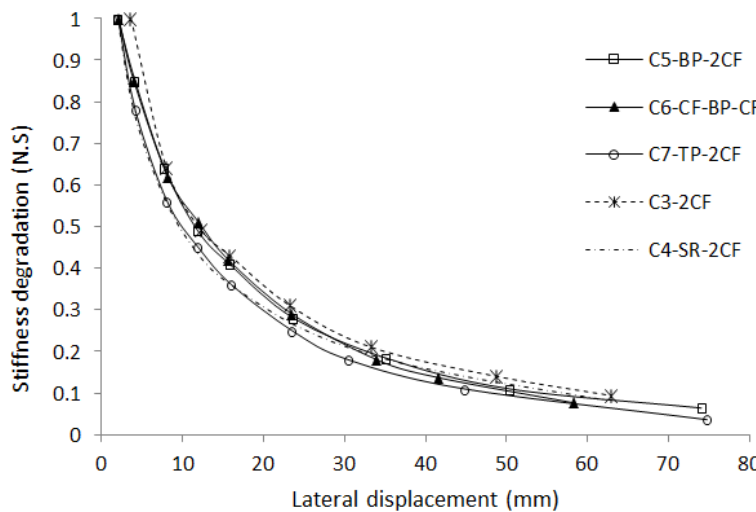
comparison with the specimens C3-2CF and C4-SR-2CF. Although T-shape steel profiles increased the yield and ultimate loads in specimen C7-TP-2CF in comparison with CFRP only strengthened specimen, the ductility factor was decreased significantly by 30.69%.

3.3 Stiffness degradation and energy dissipation

Normally, the initial stiffness of the column should not be degraded with applied cyclic loads. On the other hand, the stiffness of the structure should be large enough to control the drift ratio and be consistent with the limitation of the deformation of non-structural elements. The stiffness of each specimen was estimate using the lateral force-lateral displacement curve for both positive and negative directions. The secant stiffness is the slope of a line which connects the origin of the diagram coordinates to the point of the maximum force in the load-displacement curve in each relevant cycle of loading. The average stiffness of loading and unloading directions was considered within each cycle (Gobarah *et al.* 1997). Then, the calculated



(a) Benchmark specimens in comparison to retrofitted specimens with proposed techniques



(b) Custom retrofitted specimens in comparison to retrofitted specimens with proposed techniques

Fig. 11 Stiffness degradation curves

stiffness in each cycle is normalized to the obtained stiffness for the first cycle. The graph of the normalized stiffness (N.S) in terms of lateral displacement has been shown in Figs. 11(a)-(b). The overall behaviors of retrofitted specimens were the same; however, the specimen C5-BP-2CF had less stiffness degradation than the specimens C6-CF-BP-CF and C7-TP-2CF in the last cycles of loading. Considering normalized stiffness parameter, the specimen C1-BEN-C had less degradation than the specimen C2-BEN-UC, however, an intensive degradation has occurred in the last cycle.

The ability of a structure to survive under earthquake loading conditions depends on its ability to withstand the induced energy. Various forms of energy in the structures include kinetic energy, energy from damping, elastic energy, and hysteresis energy. A convenient way to estimate and compare the behavior of retrofitted RC columns with different retrofitting methods is to study the effects of various parameters on the energy absorption curves. The enclosed area under the hysteresis curves of the lateral load-lateral displacement has been considered as a valid criterion for calculating the amount of dissipated energy in each particular cycle of loading (Gobarah *et al.* 1997). The cumulative energy absorption of column specimens is given in Table 6. The results demonstrate that all of the strengthened specimens had a substantial improvement in inelastic response. The energy dissipation in specimens C5-BP-2CF, C6-CF-BP-CF and C7-TP-2CF were 3.58, 3.88 and 3.51 times larger than the corresponding values of the specimen BEN1 whereas this value was 2.17 and 3.17 times for specimens C3-2CF and C4-SR-2CF, respectively. The inelastic deformation is quantified generally by ductility parameter and energy absorption capacity.

For all of the specimens, the energy absorption (E.D)

graph in terms of lateral displacement is shown in Fig. 12. As shown in Fig. 12(a), the energy absorption of specimens BEN1 and BEN2 at the same displacement were almost equal. For instance, the difference in cycles 6 and 7 were about 7.6% and 3.5%, respectively. To the same extent, as the amount of accumulated energy absorption increases with increasing ultimate displacement, the responses of retrofitted specimens with composite materials will be the same. However, more increasing energy has been obtained in comparison with CFRP only strengthened specimen as an indication of appropriate seismic behavior.

4. Numerical study

The use of the finite element method, as an appropriate tool for the prediction of the behavior of structures, is a common practice in research projects (Kwon and Spacone 2002). Until now, very few studies have been carried out for the evaluation of the behavior of retrofitted RC columns with the simultaneous application of the CFRP wrapping and steel profiles, using the finite element analysis technique. Therefore a numerical study was carried out in order to evaluate the effectiveness of proposed retrofitting techniques. The finite element modeling of the columns was done using ABAQUS (ver. 2016). This software is a comprehensive program designed specifically for advanced modeling and analysis of the structures. The numerical modeling has been verified against existing experimental data. Then, the effects of important parameters, including the rebar corrosion level and the number of CFRP layers, on the structural behavior of the RC columns have been investigated.

Table 6 Cumulative energy dissipation of hysteresis curves

Specimens	C1-BEN-C	C2-BEN-UC	C3-2CF	C4-SR-2CF	C5-BP-2CF	C6-CF-BP-CF	C7-TP-2CF
Cumulated energy (KN-mm)	2869.48	2879.18	6232.08	9108.94	10264.34	11121.53	10064.44

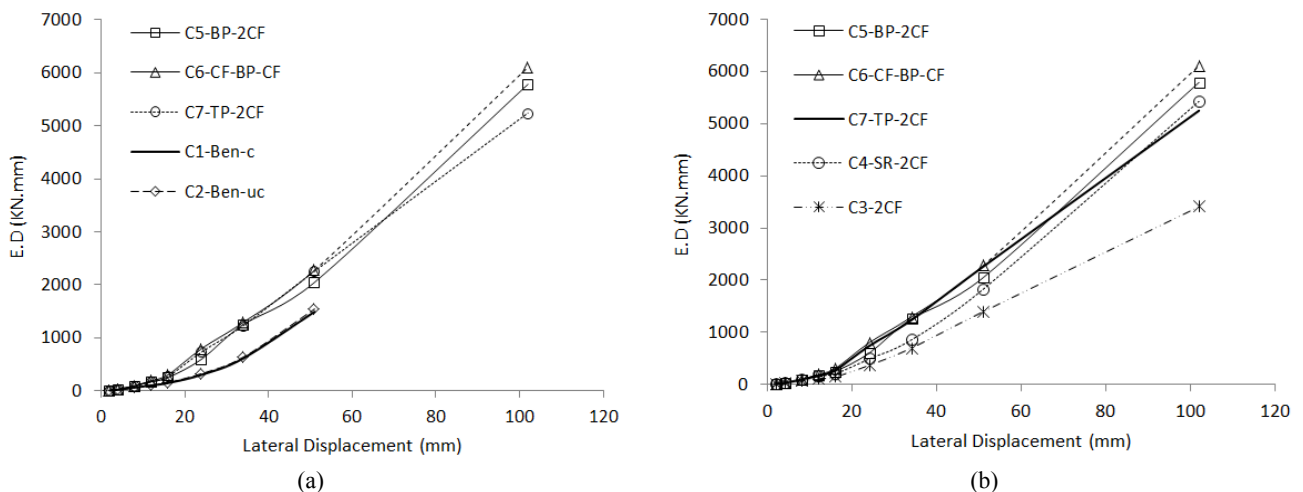


Fig. 12 Energy dissipation per lateral displacement curve

4.1 Corrosion modeling

To model the corrosion phenomenon, it is necessary to evaluate its impact on the performance of used steel rebars in the column. If the corrosion is uniform around the rebar perimeter and there are no separations in the concrete cover (“delamination” or “spalling”), then the changes in the cross-sectional area and moment of inertia of damaged area of the column will cause the significant reduction in the elastic stiffness of the RC members due to the corrosion. Conversely, it has been observed that the localized corrosion can severely affect the structural behavior and capacity of an RC element. If pitting corrosion takes place in stirrups, it could result in a reduction of confinement pressure in the concrete core and extension of the non-supported length that would lead to a premature buckling of the main rebars (Rodríguez *et al.* 1996). It has been reported that the steel ductility and strength are reduced when affected by corrosion (Lay and Schiebl 2003). The depth of penetration $p(t)$ of corrosion into the concrete surface is obtained from Eq. (4)

$$p(t) = R \cdot 0.0116 \cdot i_{corr} \cdot t \quad (4)$$

where i_{corr} is the density of current under corrosion conditions ($\mu A/cm^2$), t is the elapsed time for corrosion process (in years), R is the ratio of the maximum penetration of a pit to the average penetration corresponding to uniform corrosion (Val 2007). The parameter R , which is known as pitting ratio (Val 2007), states that the penetration of pitting corrosion into the steel reinforcement surface is about four times greater than the penetration rate under uniform corrosive conditions. Assuming that the pit is in the form of a hemisphere, the amount of reduced area is obtained for a group with n reinforcing rebars under this type of corrosion and after t years of corrosion initiation, using the following equation

$$A_s(t) = n \frac{\pi D_0^2}{4} - \sum_{i=1}^n A_{p,i}(t) \geq 0.0 \quad (5)$$

where the primary diameter of steel rebar is D_0 and $A_{p,i}(t)$ is the cross-sectional area of a pit after time t which is a function of $p(t)$. For ease of modeling, the uniform method has been selected, in which the initial cross-section and also the yield strength of steel rebars were reduced, according to Zhang *et al.* (2006). The reduction in the area of the initial cross-section of the rebars is obtained according to the Eq. (6)

$$A_D = (1 - \eta) A_0 \quad (6)$$

where A_D and A_0 are the reduced and initial cross-sectional area of rebars, respectively, and η is the corrosion ratio parameter. Another parameter for modeling of the corrosion effect is the reduction of yield strength of longitudinal and transverse steel reinforcement based on the Eq. (7) (Zhang *et al.* 2006)

$$f_{yk}^D = \frac{(1 - 1.231\eta)}{(1 - \eta)} f_{yk} \quad (7)$$

where f_{yk}^D and f_{yk} are the reduced and initial yield strength of steel reinforcement, respectively.

4.2 Finite element modeling

To model the actual behavior of the RC columns, a 3D finite element modeling has been developed. In the finite element analyses, the geometrical and material nonlinearities have been considered. As previously stated, to simulate uniform corrosion, mechanical and geometrical properties of the steel rebars have been modified. The shear deformations over the cross-section are assumed very small and negligible. Therefore, the Bernoulli hypothesis which briefly states “the plane sections remain plane after deformations” assumed to be valid, which results in linear strain distributions over the cross-section. Assuming that the bond strength between the steel rebars and concrete is maintained and the sliding does not occur, the strain in the concrete and steel rebars has proportional relation to the stress and their changes during the analysis process are linear from the neutral axis to the two upper and lower parts of the cross-section. In the preprocessing phase of the analysis, some geometric and mechanical characteristics should be defined, such as the geometric boundary conditions, the type of elements used in the FE modeling, properties of materials. For modeling of the concrete, there are various constitutive structural models. In this research, the concrete damage plasticity model is used. Solid element is a brick element type which can model the concrete members with or without rebar. This solid element has the ability to crack under tension and crushing in compression. These features, together with the rebar modeling capability, enable this element to be implemented for modeling of the concrete behavior. To model the concrete behavior, linear and nonlinear characteristics should be defined. For considering the linear isotropic behavior, the elastic modulus must be calculated according to the Eq. (8) (AASHTO LRFD 2012)

$$E_c = 33000(w_c)^{1.5} \sqrt{f'_c} \quad (8)$$

where the concrete elasticity modulus is E_c (ksi), w_c is the density of the concrete and f'_c is the compressive strength of concrete (ksi). To consider the nonlinear properties of concrete, the stress-strain relations are determined based on the model provided by Hognestad (Hognestad 1951). For modeling the nonlinear behavior of the confined concrete, the model developed by Saatcioglu and Razvi (1991) has been used. The value of the Poisson coefficient for concrete and steel was 0.2 and 0.3, respectively. For modeling the behavior of concrete under the influence of tensile stresses, it has been assumed that the stress behavior, regarding strain, has linear ratio to the uniaxial cracking stress (modulus of rupture). However, the concrete is softened beyond the uniaxial cracking stress of the concrete and due to the formation of macroscopic cracks. For modeling the concrete tensile behavior, Belarbi and Hsu’s models (1994) were used. The beam element was used for the modeling of both corrosion-damaged and un-corroded steel reinforcement. Most of the highlighted features of the beam

element are considering the plasticity, creep, rotation, simulation of bending, large deflection and large strain (Akkari and Duan 2000). The ultimate strain of the corrosion-damaged steel is obtained using the Eq. (9) (Du *et al.* 2005)

$$\varepsilon_{su(corr)} = \varepsilon_{su0}(1 - 0.005CR) \quad (9)$$

where $\varepsilon_{su(corr)}$ and ε_{su0} are the ultimate strain after corrosion and in initial state, respectively; and CR is corrosion ratio. FRP materials are microscopically un-homogeneous and anisotropic. Thus, their mechanics are more complex than conventional materials. It is assumed that the FRP sheets do not present bending stiffness. Thus the stresses in the out of plane direction are neglected.

For modeling of the CFPP sheets, a laminate element, having membrane property, has been used. The behavior of CFRP materials has been considered as orthotropic, which behaves linearly to the threshold of the failure. In addition, it has been assumed that there is no slippage between the interface of the concrete and the CFRP sheet; however, there is an adaptability of the deformation between the two elements.

4.3 Validation of FE modeling

To evaluate the accuracy and validity of the finite element modeling, it is necessary to compare the results of the numerical analysis with the reliable available experimental data carried out by other researchers. For calibration purpose, the behavior of the specimen C5-BP-2CF (in the present study) and the specimen B121 tested by Li *et al.* (2009) are used and compared with the FEM analysis results. The specimen B121 was a RC column which had a clear height of 1500 mm with a cross-section of 200 mm by 200 mm. Four 14 mm diameter bars have been used as longitudinal reinforcement; however, stirrups of 8 mm diameter bars were spaced at every 100 mm. The clear concrete cover to the hoops was 22 mm. The properties of the concrete mix and the specifications of the B121 specimen are given in Tables 7-8, respectively.

The specimen B121 has been strengthened using a combination of the CFRP sheets and steel jacket. The steel jacket consisted of four steel angles. The mechanical properties of the steel bars, steel angles, batten plates and CFRP sheets are given in Tables 9, 10 and 11, respectively.

The column has been tested under combined constant axial load and cyclic lateral displacement excursions in a test frame. Axial load was applied firstly, using hydraulic loading equipment and remained constant during the testing process to simulate the dead load on the column. The reversed cyclic lateral load has been applied using two

Table 8 Specifications of the specimen B121 (Li *et al.* 2009)

Specimen code	Corrosion loss ratio (%)	Axial load (KN)	Axial load ratio	Strengthening methos
B121	19.56	180	0.13	Steel jacket + one layer of CFRP sheet

Table 9 Mechanical properties of steel bars (Li *et al.* 2009)

Bars	Diameter (mm)	Yield stress (MPa)	Ultimate stress (MPa)
Longitudinal bar	14	384.77	604.87
Stirrups	8	326.95	510.7

Table 10 Mechanical properties of steel angle and batten plate (Li *et al.* 2009)

Element	Cross-section (mm)	Yield stress (MPa)	Ultimate stress (MPa)
Steel jacket	40×40×4	350	458.3
Batten plate	30×3	533.3	666.7

Table 11 Material properties of CFRP (Li *et al.* 2009)

Sheet thickness (mm)	Sectional area (mm ²)	Tensile strength (MPa)	Tensile modulus (MPa)	Tensile elongation (%)
0.111	1.665	3646	215,600	1.9

one-way hydraulic jacks and has been measured by two load cells attached to a hydraulic jack. Three full cycles were applied at each displacement using a triangular waveform, as shown in Fig. 13 (Li *et al.* 2009). Fig. 14 shows the numerical and experimental lateral force-lateral displacement responses of the test specimen C5-BP-2CF. The maximum lateral load and corresponding displacement as well as the degradation of shear strength and the enclosed area of curves of FE model are relatively close to those of the experimental specimen; moreover there is a reasonable match. In any case, the initial stiffness obtained in the FE analysis is slightly different from the value obtained in the experimental study.

Since the intensity of the stresses is very high at the column's base due to the existing bearing conditions, some of the flexural cracks have been formed in the initial steps of loading. By increasing the relative lateral displacement

Table 7 Properties of concrete mixing plan (Li *et al.* 2009)

Mix design	Water/cement ratio	Water (kg/m ³)	Cement (kg/m ³)	Fine aggregate (kg/m ³)	Coarse aggregate (kg/m ³)
Original concrete	0.46	205	446	526	1408
Retrofitted concrete	0.49	205	418	613	1164

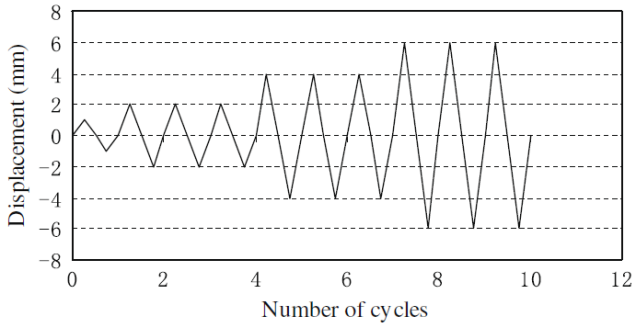


Fig. 13 Lateral displacement history (Li *et al.* 2009)

of the column, the number and size of these cracks are increased and distributed to the upper zones. A plot of Von-Mises stress distribution in the concrete, lateral deformation of the column and crack pattern variation in the steel jacket and FRP sheet are shown in Fig. 15 for the specimen C5-BP-2CF.

Fig. 16 shows the numerical and experimental lateral force-lateral displacement responses of the test specimen B121. As illustrated in this figure, the maximum lateral load, the corresponding displacement, and the degradation of lateral force have good agreement with the experimental results. The enclosed area of curves (as an energy dissipation measure) and plastic stiffness of FE curves have a little difference with those of the experimental specimen. Graphical plots of Von-Mises stress, lateral deformation of column and stress variation in the steel jacket and FRP sheet of the specimen B121 are shown in Fig. 17. Therefore, it has been found that the finite element modeling is reliable enough to be used for a parametric study about the effects of some important parameters on the behavior of retrofitted RC columns with proposed retrofitting techniques.

4.4 Parametric study

To perform a parametric study, the influences of two

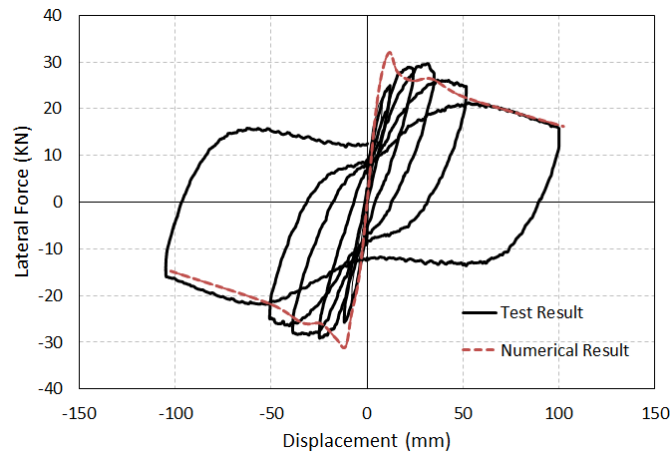


Fig. 14 Lateral force- lateral displacement curves of the specimen C5-BP-2CF; test vs. numerical result

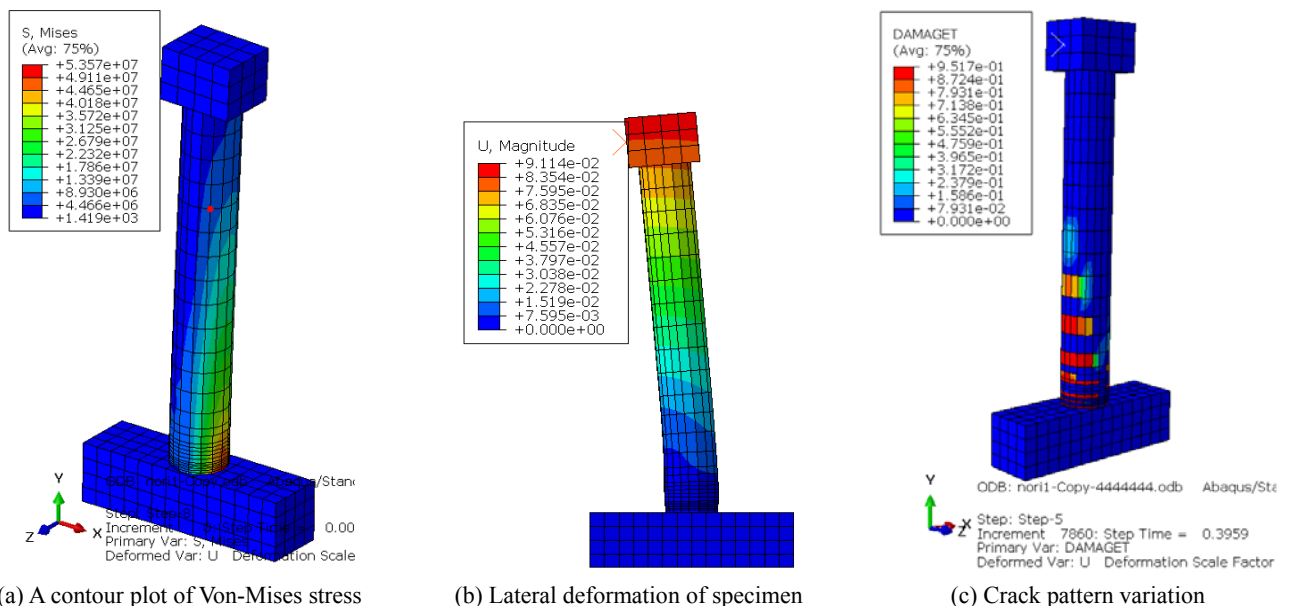


Fig. 15 Graphical plots derived from column numerical analysis

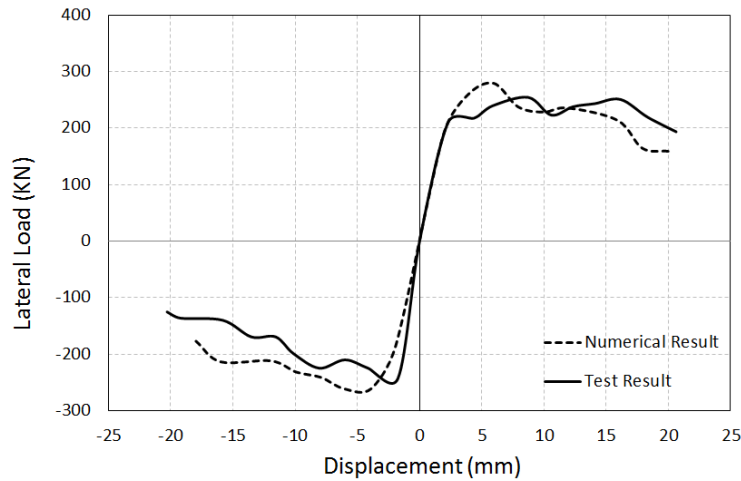


Fig. 16 Lateral force- lateral displacement curves of the specimen B121; test vs. numerical result

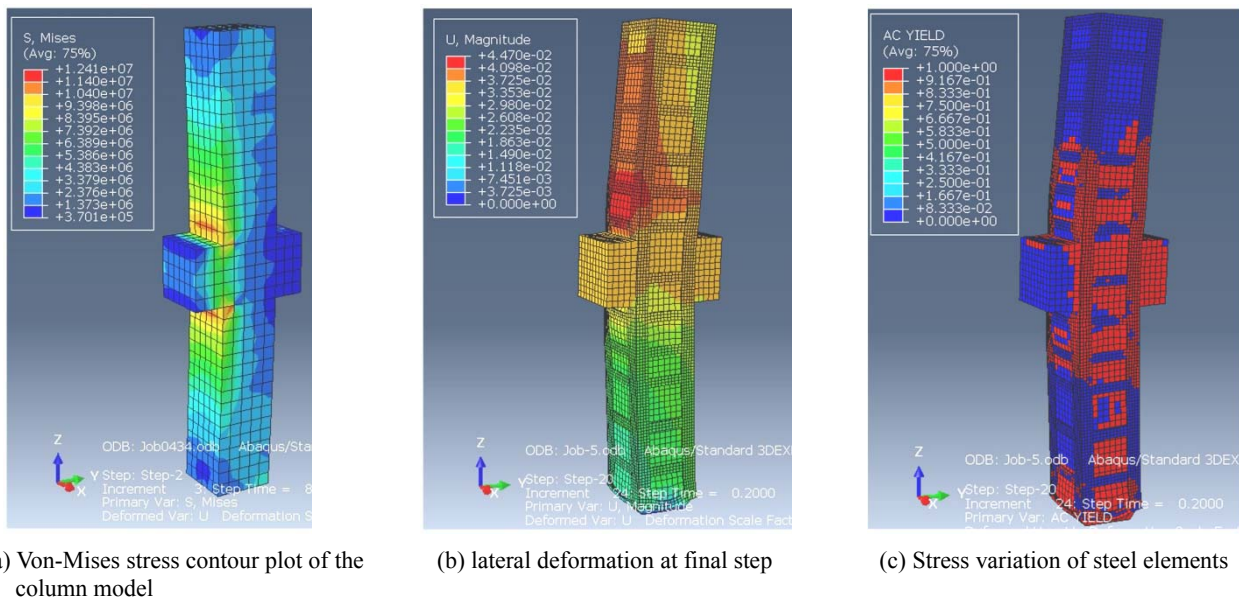


Fig. 17 Graphical plots derived from numerical analysis of test specimen B121

different parameters, namely the corrosion rate of steel rebar and the number of CFRP layers, have been studied on the behavior of retrofitted RC columns. The nonlinear geometric and material static analyses have been carried out for the prediction of the columns behavior. The benchmark model had the specifications of the retrofitted specimen C5-BP-2CF (introduced in the present study), except that the compressive strength of the concrete is assumed to be $f_c = 20$ Mpa and also the RC column model was not corroded (degree of corrosion = 0%). For evaluation of the effects of each parameter, the hysteresis curves of the benchmark model and the other models have been compared. It is worth noting that the envelope curve is drawn based on the amount of shear strength and related lateral displacement in the turning point of each cycle in both loading and unloading directions.

4.4.1 Effect of the corrosion rate of steel rebars

The corrosion rate of steel rebars has a considerable

effect on the structural behavior of the retrofitted RC columns. Four rates of corrosion, 2%, 4%, 6% and 8% have been considered. Fig. 18 illustrates the lateral load-lateral displacement curves of the models with different rates of steel rebar corrosion. When the rate of corrosion is low, the overall behavior will be similar. As shown in Table 12, higher corrosion level results in less lateral capacity in corroded RC column model. As the corrosion rate of the rebars increases, the cross-sectional area of the rebars will be decrease, which causes the reduction of yield strength of the column rebars. The result of these changes is the buckling of the longitudinal rebars that are subjected to the compressive stress, causing the less lateral load carrying capacity of the column. For instance, the maximum lateral loads are 61.60 kN and 53.40 kN and the ductility factors are 5.97 and 6.27, under the rates of corrosion 2% and 8%, respectively, showing more ductile behavior under a higher rate of rebar corrosion. As illustrated in Fig. 19, the maximum Von-Mises stress is appeared in the lower part of

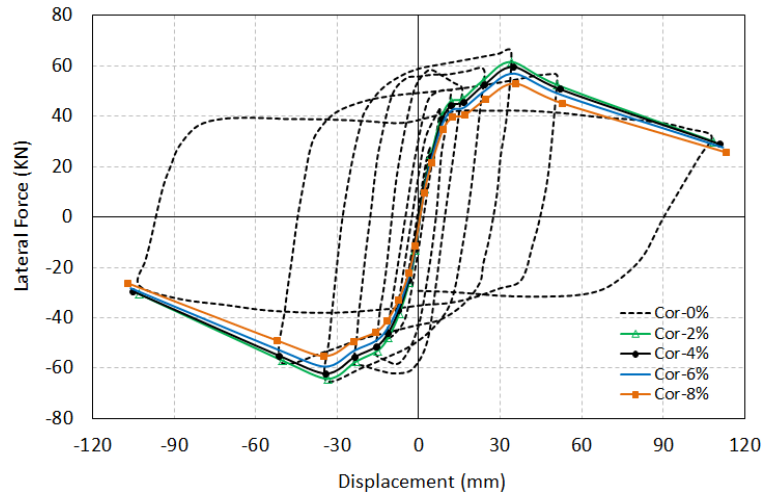


Fig. 18 The lateral load-lateral displacement curves of the models with different rates of steel rebar corrosion

Table 12 The effects of corrosion rate on the ductility and maximum lateral load of the columns

Parameters/Specimens	0%	2%	4%	6%	8%
Maximum lateral load (KN)	65.66	61.60	59.42	57.12	53.40
Ductility	5.89	5.97	6.09	6.17	6.27

the column (corrosion rate is 8%). However, the plastic hinge formation has initiated at the lowest part and propagated towards the upper part of the model. Prior to the crushing of the column concrete cover, yielding of tensile steel rebars has been initiated. Therefore, the column has experienced a flexural-shear failure. At the seventh cycle, considerable flexural cracks were appeared on the surface of the CFRP sheet in both directions around the plastic hinge region and propagated until the failure of column.

4.4.2 The effect of the number of CFRP layers

The thickness of the CFRP sheets has a significant effect on the structural behavior of the retrofitted columns. The effect of thickness can also appear in the form of the number of CFRP layers. In this study, the number of applied layers was one, two, three and four. In Fig. 20, the lateral force-lateral displacement response curves are shown, considering the effect of the number of CFRP layers. The retrofitted model with one layers of CFRP sheet shows a more unstable hysteresis response, which is due to the lower amount of the confinement pressure on the concrete core. Therefore, a decrease is observable in the amount of lateral strength and ductility. As the number of CFRP layers increases, the confinement level in the plastic hinge region will improve, resulting in better performance under reversed cyclic displacement. As a result, the formation of internal cracks is delayed between the corrosion-damaged column and the steel jacket and the bond resistance will improve. The energy dissipation in each cycle per related displacement for each model is shown in Fig. 21. It is noteworthy

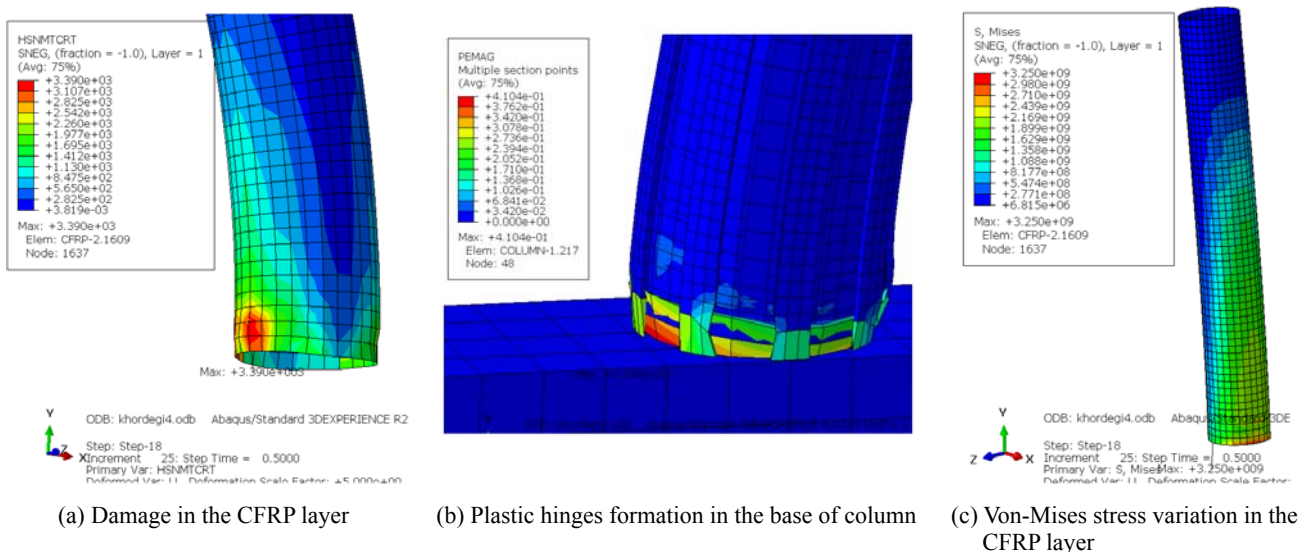


Fig. 19 Graphical plots at the end step of FE analyses

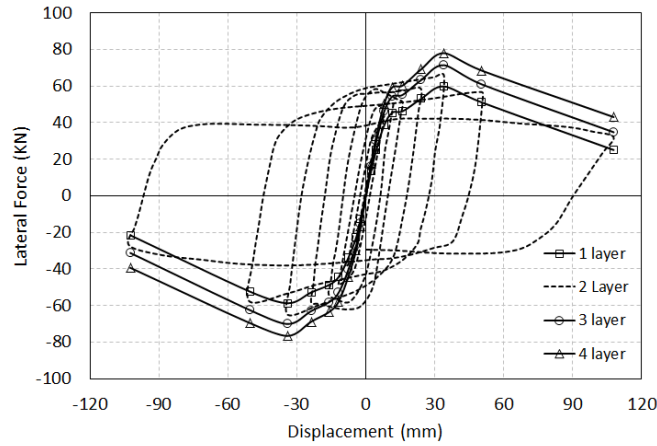


Fig. 20 Effect of number of the CFRP layers on the lateral load–displacement curves

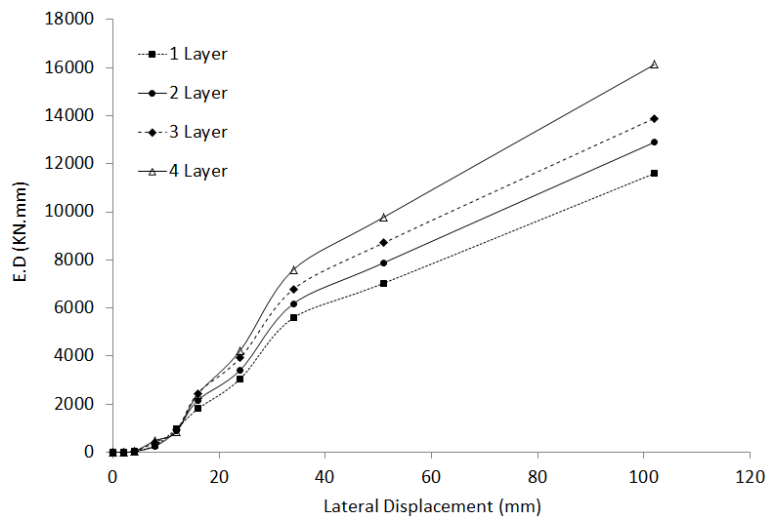


Fig. 21 Effect of number of CFRP layers on the energy dissipation of column models

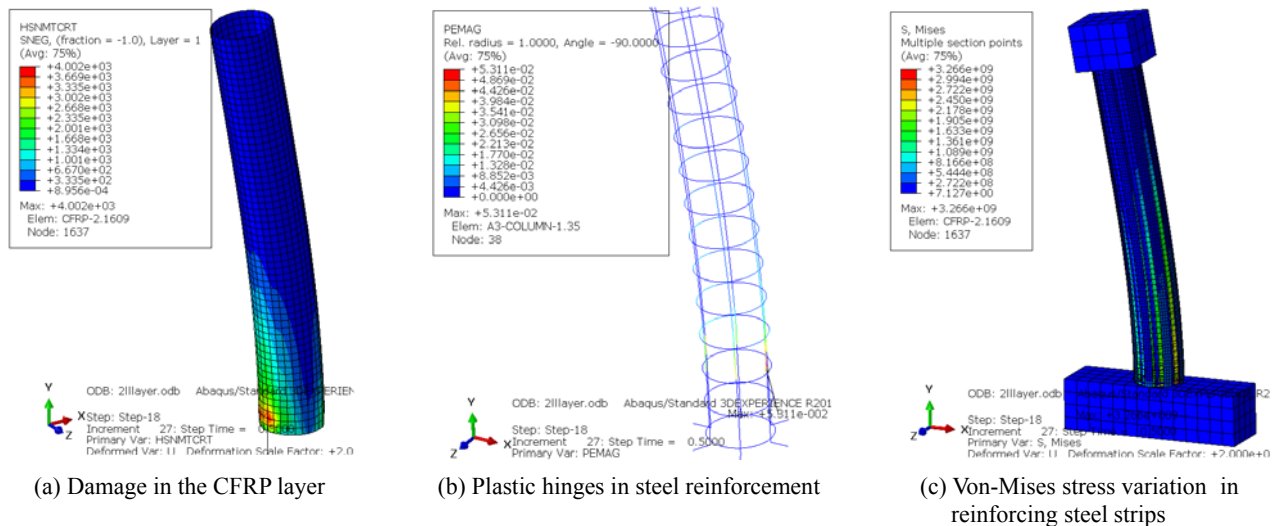


Fig. 22 Graphical plots at the end step of FE analyses

that the energy dissipation of the RC column model increases by increasing the layers of CFRP. As a comparison, the amount of this parameter is 5598.5 KN.mm

and 7597.5 KN.mm for the models with one and four layers of CFRP in the seventh cycle of loading, respectively. The plastic hinge formation of steel reinforcement in Fig. 22 is

an indication of yielding of reinforcing rebars, causing the flexural-shear failure of the column (having two layers of CFRP).

5. Conclusions

A numerical and experimental study has been carried out on the seismic behavior of RC bridge columns, damaged under corrosive environments and retrofitted by combined application of CFRP sheets and steel profiles. Seven scaled RC column specimens of a Girder Bridge were tested under the application of axial load and cyclic lateral displacements. Also, a numerical study was carried out using finite element analysis technique. At first, the accuracy of the finite element modeling was checked using the results of two experimental models. Then the effects of parameters such as the corrosion rate of steel rebars and the number of CFRP layers have been investigated using ABAQUS software. Some important results of the present research are as follows:

- Retrofitting of the corroded RC columns with a combination of the CFRP wrapping and steel profiles causes the significant improvement in the strength as well as cumulative energy dissipation under cyclic lateral load in comparison to retrofitting work with only single material such as CFRP wrapping technique. However, their average normalized stiffness degradations are close enough to each other.
- Although the displacement ductility factor of the specimen, retrofitted using inner steel strips and outer CFRP layers, has the highest value; but two remained specimens, retrofitted using the outer CFRP layers and inner steel strips; and also inner T-shape steel profiles and outer CFRP layers, showed lower amount in the ductility parameter compared to the specimen retrofitted only with CFRP sheets.
- The effects of the rate of the longitudinal and transverse rebars corrosion are very significant on the structural behavior of the retrofitted RC columns. Higher corrosion rate leads to more stiffness degradation, more reduction in the displacement ductility factor and also in energy dissipation parameter. However, the degradation of maximum lateral force in each cycle of the hysteresis curves happened faster.

When the number of CFRP layers increases, the lateral strength and energy absorption capacity of retrofitted RC columns will improve. However, increasing the number of CFRP layers can lead to less ductility in retrofitted RC columns.

References

AASHTO LRFD (2012), *Bridge Design Specifications*, American Association of State Highway and Transportation Officials; DC, USA.
 ABAQUS (2016), *ABAQUS/CAE User's Manual*; Dassault Systèmes Simulia Corp., Providence, RI, USA.

Abdullah, V. and Katsuki, T. (2003), "An investigation into the behavior and strength of reinforced concrete columns strengthened with ferrocement jackets", *Cement Concrete Compos.* **25**(2), 233-242.
 Adam, J.M., Giménez, E., Calderón, P.A., Pallarés, F.J. and Ivorra, S. (2008), "Experimental study of beam-column joints in axially loaded RC columns strengthened by steel angles and strips", *Steel Compos. Struct., Int. J.*, **8**(4), 329-342.
 Adam, M., Ivorra, S., Pallares, F., Gimenez, E. and Calderon, P. (2009), "Axially loaded RC columns strengthened by steel casing: finite element modeling", *Constr. Build. Mater. J.*, **161**, 337-348.
 Akkari, M. and Duan, L. (2000), *Nonlinear Analysis of Bridge Structures*, Bridge Engineering Handbook, (Ed. Wai-Fah Chen and Lian Duan), Boca Raton, CRC Press.
 Andisheh, K., Scott, A. and Palermo, A. (2016), *Seismic Behavior of Corroded RC Bridge*, International Journal of Corrosion, Hindawi Publishing Corporation.
 Anoop, M.B. and Rao, K.B. (2015), "Seismic damage estimation of reinforced concrete framed structures affected by chloride-induced corrosion", *Earthq. Struct., Int. J.*, **9**(4), 851-873.
 Aquino, W. and Hawkins, N.M. (2007), "Seismic retrofitting of corroded reinforced concrete columns using carbon composites", *ACI Struct. J.*, **104**(3), p. 348.
 Architectural Institute of Japan (1987), Data on ultimate strength design of reinforced concrete structures; Report No. 17, Strength and Ductility of Reinforced Concrete Columns, Tokyo, Japan, pp. 62-85.
 Badalamenti, V., Campione, G. and Mangiavillano, M. (2010), "Simplified model for compressive behavior of concrete columns strengthened by steel angles and strips", *Eng. Mech. J. ASCE*, **136**, 230-238.
 Barga, F., Gigliotte, R. and Laterza, M. (2006), "Analytical stress-strain relationship for concrete confined by steel stirrups and/or FRP jackets", *Struct. Eng. J.*, **9**, 2-19.
 Belarbi, A. and Hsu, T.T. (1994), "Constitutive laws of concrete in tension and reinforcing bars stiffened by concrete", *Struct. J.*, **91**(4), 465-474.
 Campione, G. (2012), "Load carrying capacity of RC compressed columns strengthened with steel angles and strips", *Eng. Struct. J.*, **40**, 457-465.
 Carins, J., Plizzari, G., Du, Y., Law, D. and Franzoni, C. (2005), "Mechanical properties of corrosion reinforcement", *ACI Mater. J.*, **102**(4), 256-264.
 Chen, H.P. and Xiao, N. (2015), "Symptom-based reliability analyses and performance assessment of corroded reinforced concrete structures", *Steel Compos. Struct., Int. J.*, **53**(6), 1183-1200.
 Choi, E., Rhee, I., Park, J. and Cho, B.S. (2011), "Seismic retrofit of plain concrete piers of railroad bridges using composite of FRP-steel plates", *Compos.: Part B*, **42**, 1097-1107.
 Debaiky, A.S., Green, M.F. and Hope, B.B. (2006), "Long-Term monitoring of carbon fiber-reinforced polymer-wrapped reinforced concrete columns under severe environment", *ACI Struct. J.*, **103**(6).
 Dionysios, A., Bournas, C. and Triantafillou, C. (2009), "Flexural strengthening of reinforced concrete columns with Near-surface-Mounted FRP or Stainless Steel", *ACI Struct. J.*, **106**(4).
 Du, Y.G., Clark, L.A. and Chan, A.H.C. (2005), "Residual capacity of corroded reinforcing bars", *Magaz. Concrete Res.*, **57**(3), 135-147.
 Fookers, P. (1995), "Concrete in hot dry salty environment", *Concrete*, **29**(1), 34-39.
 Gao, S., Ikai, T., Ni, J. and Ge, H. (2016), "Load-carrying capacity degradation of reinforced concrete piers due to corrosion of wrapped steel plates", *Steel Compos. Struct., Int. J.*, **20**(1), 91-106.

- Gao, S., Ni, J., Zhang, D. and Ge, H. (2017), "Strength degradation of reinforced concrete piers wrapped with steel plates under local corrosion", *Steel Compos. Struct., Int. J.*, **24**(6), 753-765.
- Gobarah, A., Biddah, A. and Mahgoub, M. (1997), "Rehabilitation of reinforced concrete columns using corrugated steel jacketing", *J. Earthq. Eng.*, **4**(1), 651-673.
- Goksu, C. (2012), "Seismic behavior of RC columns with corroded plain and deformed reinforcing bars", Ph.D. Dissertation; Istanbul Technical University, Turkey.
- Gong, J., Zhong, W. and Zhao, G. (2004), "Experimental study on low-cycle behavior of corroded reinforced concrete member under eccentric compression", *J. Build. Struct.*, **25**(5), 92-104.
- Greco, R. and Marano, G.C. (2015), "Strength deterioration of reinforced concrete column sections subject to pitting", *Comput. Concrete, Int. J.*, **15**(4), 643-671.
- Hognestad, E. (1951), "A study of combined bending and axial load in reinforced concrete members", Bulletin No. 399; Univ. of Illinois, Eng. Experimental Station, Champaign, IL, USA.
- Husain, M., Mohamed, H. and Ahmed, S. (2017), "Evaluation of non-conforming corroded bridge piers exposed to seismic loads", *Int. J. Eng. Innov. Technol.*, **7**(3).
- Kwon, M. and Spacone, E. (2002), "Three-dimensional finite element analysis of reinforced concrete columns", *Comput. Struct.*, **80**, 199-212.
- Lay, S. and Schiebl, P. (2003), "Life cycle management of concrete infrastructures for improved sustainability", *European Community Fifth Framework program*, GROWTH.
- Lee, C., Bonacci, J.F., Thomas, M.D., Maalej, M., Khajehpour, S., Hearn, N., Pantazopoulou, S. and Sheikh, S. (2000), "Accelerated corrosion and repair of reinforced concrete columns using CFRP sheets", *Can. J. Civil Eng.*, **27**(5), 949-959.
- Lee, H.S., Kage, T., Noguchi, T. and Tomosawa, F. (2003), "An experimental study on the strengthening effects of reinforced concrete columns damaged by rebar corrosion strengthened with carbon fiber sheets", *Cement Concrte Res.*, **33**(4), 563-570.
- Li, J., Gong, J. and Wang, L. (2009), "Seismic behavior of corrosion-damaged reinforced concrete columns strengthen using combined carbon fiber-reinforced polymer and steel jacket", *J. Constr. Build. Mater.*, **23**, 2653-2663.
- Lu, Y.Y., Chen, S.X. and Zhao, G.F. (2005), "An experimental study on the seismic behavior of reinforced concrete column strengthened with bonded steel hoops and carbon fiber reinforced polymer sheet", *China Civil Eng. J.*, **38**(8), 10-7.
- Ma, Y., Che, Y. and Gong, J. (2012), "Behavior of corrosion damaged circular reinforced concrete columns under cyclic loading", *Constr. Build. Mater.*, **29**, 548-556.
- Maaddawy, T. (2008), "Behavior of corrosion-damaged RC columns wrapped with FRP under combined flexural and axial loading", *Cement Concrte Compos.*, **30**(6), 524-534.
- Malerba, P.G., Sgambi, L., Ielmini, D. and Gotti, G. (2017), "Influence of corrosive phenomena on bearing capacity of RC and PC beams", *Adv. Concrete Constr., Int. J.*, **5**(2), 117-143.
- Mangat, P.S. and Elgarf, M.S. (1999), "Bond characteristics of corroding reinforcement in concrete beams" *Mater. Struct.*, **32**(2), 89-97.
- Meda, A., Mostosi, S., Rinaldi, Z. and Riva, P. (2014), "Experimental evaluation of the corrosion influence on the cyclic behavior of RC column", *Eng. Struct.*, **76**, 112-123.
- Montuori, R. and Piluso, V. (2009), "Reinforced concrete columns strengthened with angles and battens subjected to eccentric load", *Eng. Struct. J.*, **31**(2), 539-550.
- Nakayama, K., Yamakawa, T., Iraha, S. and Biwasa, A. (1995), "An experimental study on plastic behavior of reinforced concrete columns corroded in electrolytic corrosion test", *Proc. Jpn. Concr. Inst. Annu. Conf*, **17**(1), 883-888.
- Pantazopoulou, S.J., Bonacci, J.F., Sheikh, S., Thomas, M.D.A. and Hearn, N. (2001), "Repair of corrosion-damaged columns with FRP wraps", *J. Compos. Constr.*, **5**(1), 3-11.
- Ranjith, A., Balaji, K. and Manjunath, K. (2016), "Evaluating the effect of corrosion on service life prediction of RC structures- A parametric study", *Int. J. Sustain. Built Environ.*, **5**, 587-603.
- Ramirez, L., Barcena, M., Urreta, I. and Sanchez, A. (1997), "Efficiency of short steel jackets for strengthening of square section concrete column", *Constr. Build. Mater. J.*, **11**(5), 45-52.
- Rodriguez, J., Ortega, L.M. and Casal, J. (1996), "Load bearing capacity of concrete columns with corroded reinforcement; Corrosion of reinforcement in concrete construction", Royal Society of Chemistry, pp. 220-230.
- Saatcioglu, M. and Razvi, S. (1991), "Analytical model for confined concrete", Research Report No. 9101: Dept. of Civil Engineering, University of Ottawa, Ottawa, ON, Canada, 59.
- Sasmal, S., Ramanjaneyulu, K., Novák, B., Srinivas, V., Kumar, K.S., Korkowski, C., Roehm, C., Lakshmanan, N. and Iyer, N.R. (2011), "Seismic retrofitting of nonductile beam-column sub-assembly using FRP wrapping and steel plate jacketing", *Constr. Build. Mater.*, **25**, 175-182.
- Sheikh, S.A. and Yau, G. (2002), "Seismic behavior of concrete columns confined with steel and fiber-reinforced polymers", *ACI Struct. J.*, **99**(1), 72-80.
- Tastani, S.P. and Pantazopoulou, S.J. (2004), "Experimental evaluation of FRP jackets in upgrading RC corroded columns with substandard detailing", *Eng. Struct.*, **26**, 817-829.
- Val, D.V. (2007), "Deterioration of strength of RC beam due to corrosion and its influence on beam reliability", *J. Struct. Eng.*, **133**(9), 1297-1306.
- Vandoros, K.G. and Dritsos, S.E. (2008), "Concrete jacket construction detail effectiveness when strengthening RC columns", *Constr. Build. Mater.*, **22**(3), 264-276.
- Wang, X. (2004), "Research of seismic Performance and Hysteretic Mode of Corroded Reinforced Concrete", Members Master; Xi'an, China.
- Yu, K., Huang, T. and Lu, L.W. (1989), "Design, analysis and experiment planning of one-story reinforced concrete frame-wall-diaphragm assemblage", Fritz Engineering Laboratory Library; Department of Civil Engineering, Leigh University, Bethiehem, PA, USA.
- Yuksel, I. (2015), "Rebar corrosion effects on structural behavior of building", *Struct. Eng. Mech., Int. J.*, **54**(6), 1111-1133.
- Zhang, W.P., Shang, D.F. and Gu, X.L. (2006), "Stress-strain relationship of corroded steel bars", *J. Tongji Univ. (Natural Scienc)*, **34**(5), 586-592.